JOURNAL OF MATERIALS SCIENCE 31 (1996) 1575–1584

Cracking orientation and induced anisotropy of a ceramic matrix composite under off-axis loading

S. BASTE, R. EL BOUAZZAOUI
Université Bordeaux I, U.R.A. C.N.R.S. no. 867, Laboratoire de Mécanique Physique, 351, Cours de la Libération, 33405-TALENCE Cedex, France

The effect of matrix microcracking on the stiffnesses of a carbon-fibre/SiC-matrix woven composite is studied by means of an ultrasonic method. It provides the whole set of the stiffness tensor coefficients which are inaccessible by classical strain measurements and which are required to identify anisotropic damage. The induced anisotropy depends on the loading direction. If a tensile solicitation in a fibre direction leads to stiffnesses decreases without any rotation of principal axes, a tensile solicitation of 45° from a fibre direction creates microcracks with a predominant orientation that does not coincide with the elastic symmetry axes, and induce a fully anisotropic elastic degradation.

1. Introduction

Matrix cracking is the fundamental mechanism of deformation in ceramic matrix composites [1–4]. The most remarkable effects of the growth of the microcracks are the non-linearity in the stress–strain relationship, and the degradation of elastic stiffnesses. Most studies of damage in these materials have been concerned with the failure and toughness aspects, to understand the damage process and to obtain the condition (failure criteria) for crack propagation [1–7]. Another group of investigations relies on the prediction of the stiffness reduction in a body containing cracks [8–15].

This point of view, which may be termed micromechanics, implied that the nature of damage is identified and described geometrically. It is also true for the ideal representation of cracks used in the various truncations existing in the literature [16–21] of the general description of damage [22]. If the damage is defined as the change of the elasticity tensor [22], no preliminary knowledge of the microstructure is required. The interest in this description of damage lies in its generality and in its purely phenomenological character. The price to pay for its simplicity is that the variations of the whole stiffness tensor must be studied. If classical measurement methods lead to a partial identification of these tensor variations, an ultrasonic device connected to a tensile machine makes it possible to perform the measurements of the nine stiffness coefficients, describing completely the elasticity of an orthotropic material during a tensile test [23, 24]. Since the general definition of the damage agrees with analytical results of the micromechanical approaches, comparison of experimental measures of damage carried out without *a priori* crack geometry with theoretical predictions of the changes in elasticity coefficients deduced from an ideal representation, allows identification of the approximate orientation of the microcracking.

This paper treats the damage induced anisotropy that is orientation of matrix cracks as a function of the loading direction and to the natural axes of the composite. In composite materials, the microcracks have a preferential orientation. Their effect is highly anisotropic. Anisotropy arises because failure mechanisms favour the generation of microcracks oriented normal to the tensile stress. Only a damage field that is parallel to one of the three orthogonal axes of material symmetry preserves the orthotropic symmetry in the elastic coefficients. This is the case when the composite is submitted to a tensile stress in one of the fibre directions. The damage process is then a matrix cracking which propagates perpendicular to the fibres that are aligned with the tensile loading direction. The directions of cracks' growth are in respect with the bi-directional texture of the composite; the material keeps its orthorhombic symmetry during the degradation process. In contrast, an off-axis solicitation creates microcracks with a predominant orientation that may depend on the loading direction or on the fibre directions. If the cracks' orientation does not coincide with the fibre axes, it induces a fully anisotropic elastic degradation. The measurement of the change of all the stiffness tensor components during a damaged process is done for a 2D carbon–SiC composite material submitted first to a tensile test in one of the fibre directions and second to a tensile solicitation 45° from the fibre directions.

2. Material and experimental procedure

2.1. Material

The material studied is a bi-directional carbon–SiC composite prepared by S.E.P (Société Européenne de Propulsion, France). It is fabricated from a 2D fibrous

0022–2461

preform built up from multiple layers of carbon cloths. The SiC matrix was added by a chemical vapour infiltration (CVI) process. Before infiltration of the matrix, the carbon fibres were coated with a pyrocarbon interphase of mean thickness of about 1 μm to enhance the desired non-catastrophic tensile behaviour [25]. These processing steps resulted in a material having a density close to 2 $g\,cm^{-3}$, a fibre content of approximately 40 vol % and a residual porosity inherent to the CVI process in the range 10–15%.

Because of its bi-directional structure, the material possesses three perpendicular planes of symmetry and it satisfies the hypothesis of an orthorhombic symmetry required by the ultrasonic technique.

Two samples referred to as S0 and S45, in the form of plates measuring 190 mm × 50 mm × 3 mm, are used in this study. Sample S0 is cut out according to the cloths' axes and S45 according to a 45° angle from fibre axes. Samples S0 and S45 have been extracted from two different plates of material.

2.2. Ultrasonic evaluation of the stiffness tensor

The main principles and the methods of ultrasonic non-destructive evaluation (NDE) have been given by Roux [26] for the recovery of the elastic constants of anisotropic materials. Ultrasonic evaluation makes it possible to measure the nine stiffness coefficients describing completely the elasticity of an orthorhombic material.

The ultrasonic characterization purpose is to solve the inverse problem of Equation [27]:

$$\det(\Gamma_{ij} - \rho v^2 \delta_{ij}) = 0, \text{ with}$$

$$\Gamma_{ij} = C_{ijkl} n_k n_l, \quad i, j = 1, 2, 3, \qquad (1)$$

where ρ is the density, **n** is the direction of propagation, v is the velocity, C_{ijkl} are the elasticity coefficients and δ_{ij} is Kronecker's delta function. Stiffnesses are recovered as the coefficients of Equation 1 from suitable sets of experimental values of its roots ρv^2 in various directions **n** [28]. This recovery of the stiffness coefficients from the experimental velocities is solved by an optimization inversion method. It minimizes, in the least square sense, the shift between the experimental values, and the one calculated from Equation 1 for the optimum values of the stiffnesses. For a thin plate sample, the measurements made in the two accessible principal planes lead to the identification of seven coefficients of the stiffness tensor, namely: C_{11}, C_{22}, C_{12}, C_{66} for a propagation in the plane (1, 2) (in axes of Fig. 1), and C_{11}, C_{33}, C_{13}, C_{55} in the plane (1, 3). The two remaining coefficients C_{23} and C_{44} are identified using the previously identified coefficients by propagation in the non-principal plane of symmetry (1, 45°) of orthorhombic materials [29]. Axis 45° is defined as the bisecting line of the axes 2 and 3 (see Fig. 1). For tetragonal material, this plane is a plane of symmetry and those two stiffnesses can not be measured independently [30]. The value of C_{44} is measured with contact transducers. The value of C_{23} is recovered in the plane (1, 45°).

Wave speed measurements are performed by using ultrasonic pulses which are refracted through a plate sample immersed in water [31]. Because of the signal distortion due to the propagation in a porous medium [32], a special signal processing method was developed [33]. It leads to the correct measurement of the phase velocity of the pulses through the porous sample. An estimation of the confidence interval associated with each identified constant is calculated [34] by means of a statistical analysis of the set of the velocity measurements in each plane of propagation.

The stiffnesses of the sample S0 before load, in the coordinate axes placed on the cloths' axes, Fig. 1, and their 90% confidence interval are:

$$[C_{ij}] = \begin{bmatrix} 19 \pm 2 & 7.9 \pm 0.6 & 7.7 \pm 0.3 & & & \\ & 118 \pm 7 & 23 \pm 30 & & & \\ & & 123 \pm 4 & & & \\ & & & 23 \pm 2 & & \\ & \text{Sym.} & & & 8.5 \pm 0.2 & \\ & & & & & 9.1 \pm 0.1 \end{bmatrix} \text{ in GPa}$$

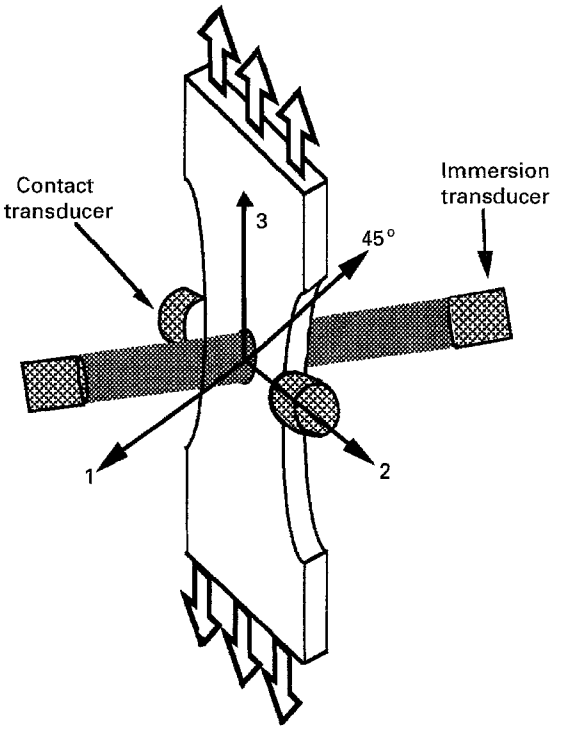

Figure 1 Under load ultrasonic device. Sample is scanned in three planes; the principal plane (1, 3) defined by the normal to the plate and the fibre direction, the principal plane (1, 2) and the non-principal plane (1, 45°), axis 45° being defined as the bisecting line of the axes 2 and 3.

The carbon cloths are balanced weaves. So, the directions 2 and 3 are symmetrically equivalent. Certain stiffnesses are equal: $C_{22} \approx C_{33}, C_{66} \approx C_{55}$, $C_{12} \approx C_{13}$. The carbon–SiC 2D composite presents a tetragonal symmetry with six independent stiffnesses.

3. Stiffness tensor changes under tensile loading in one of the fibre directions

An immersion ultrasonic tank associated with a tensile machine composes the under load characterization device [23, 24]. It makes it possible to perform, under load, the angular investigation in the three planes required to identify the elasticity tensor [29].

3.1. Stiffness tensor changes

Sample S0 has been submitted to a tensile test in direction 3 which is parallel to one of the fibres' directions. The loading was applied in 20 steps of stress, necessary for the ultrasonic evaluation, until the sample failed at 360 MPa. Fig. 2 plots the change of the nine independent stiffnesses and their confidence interval identified from the phase velocities as a function of tensile stress.

The 2D carbon–SiC composite does not exhibit an elastic behaviour. The stiffness coefficients decrease from the outset of the loading. We note an important loss of stiffness along the tensile axis (axis 3), from 123 to 75 GPa. On the other hand, C_{22} is essentially constant. The cracks grow preferentially in the plane transverse to the loading direction [14]. It is worth noting that the microcracking also affects the shear moduli, and particularly those relative to the planes that contain the loading direction, i.e. C_{44} and C_{55}. The 40% decrease of the in-plane shear modulus C_{44} is quite similar to the decrease of C_{33}. The microcracking does not affect perceptibly the elasticity coefficients C_{22}, C_{12} and C_{66} of plane (1, 2) normal to the fibres. Only the stiffnesses C_{33}, C_{13}, C_{23}, C_{44} and C_{55} of planes including the loading axis are modified.

The damage induced anisotropy involves a change in the symmetry of the composite. The predominant orientation of the microcracks destroys the balance of the carbon cloths. The directions 2 and 3 are no longer symmetrically equivalent under load. The elastic symmetry, which was initially tetragonal, becomes increasingly orthorhombic: $C_{22} \neq C_{33}$, $C_{66} \neq C_{55}$, $C_{12} \neq C_{13}$.

3.2. Tridimensional description of non linear behaviour

The microcracking affects the physical and mechanical properties. Degradation of one of those properties

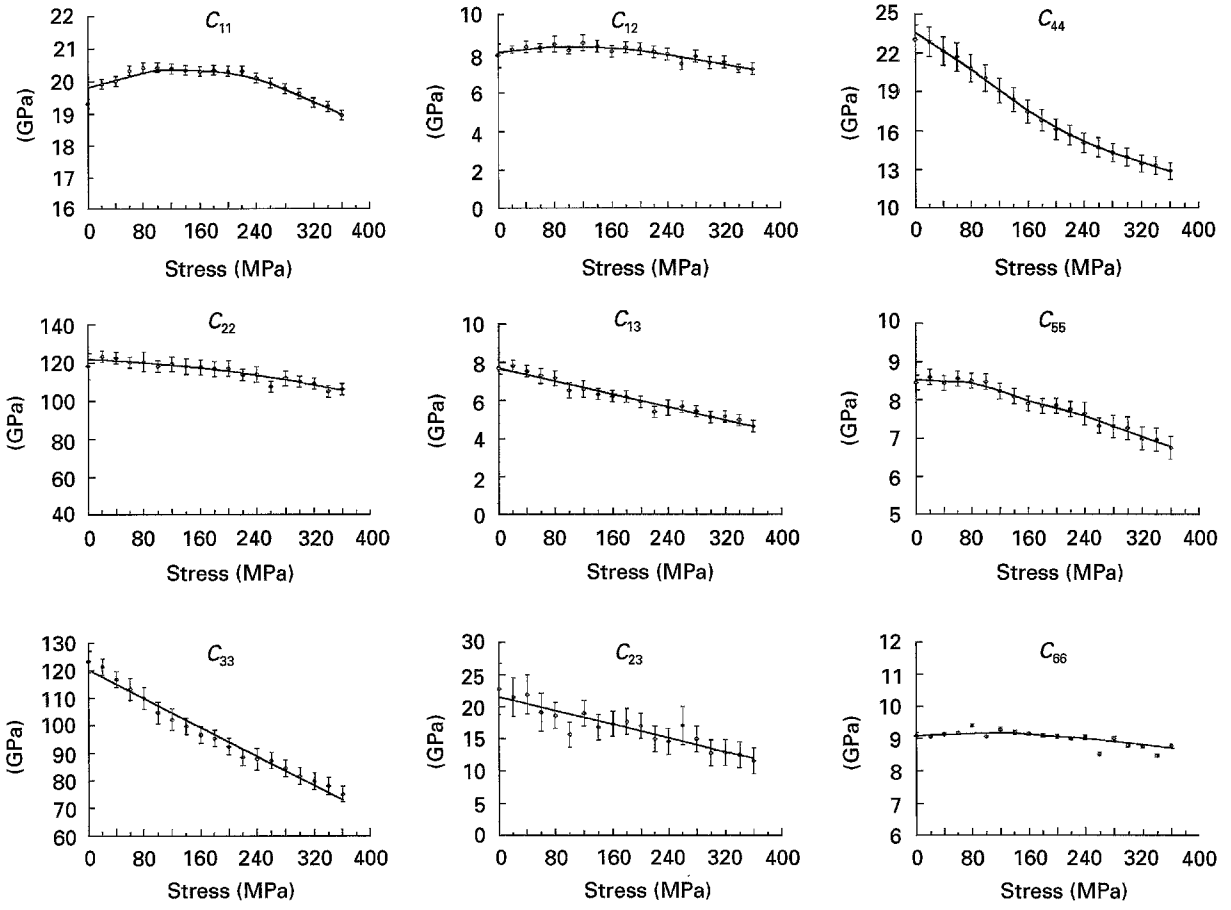

Figure 2 Variation of the stiffness tensor coefficients and their 90% relative confidence interval with the tensile stress in one of the fibre directions, direction 3, sample S0.

is an indirect measurement of damage. Changes in the values of the elastic stiffnesses can be taken as a characterization of the state of damage of the material [35]. The elasticity tensor can be written in an additive form [36]:

$$\mathbf{C} = \mathbf{C}_0 - \mathbf{C}_c \quad (2)$$

in terms of the stiffness tensor $\mathbf{C}_0$ of the uncracked material and of the loss of stiffness $\mathbf{C}_c$ due to the microcracks. The variation of the stiffness tensor:

$$\omega = \mathbf{C}_c = \mathbf{C}_0 - \mathbf{C} \quad (3)$$

is selected as an internal variable representing the current state of the microcracking of the material. Like the initial elasticity tensor C_0, the effective stiffness is a fourth rank symmetrical tensor, and the damage variable ω shows the same properties. With the introduction of usual abbreviated subscript notation, Equation 3 becomes:

$$\omega_{IJ} = C^0_{IJ} - C_{IJ} \qquad I, J = 1 \text{ to } 6 \quad (4)$$

The components of this tensor have a clearly identifiable physical meaning, and they form a finite set of data and a fully anisotropic behaviour can be described.

Traditionally, in phenomenological models based on the thermodynamics of continuous media, the damage parameter varies from zero for the initial state to the critical value $d = 1$ at the failure of the volume element [37]. To this end it is necessary to normalize the components of the damage tensor to their thermodynamically admissible maximum values $\omega^{\lim}_{IJ}$ such that the elasticity tensor remains a definite positive operator, i.e. the volume free energy of the damaged material is still positive [22]. The components of the normalized damage tensor are then given by:

$$D_{II} = \frac{\omega_{II}}{\omega^{\lim}_{II}} = 1 - \frac{C_{II}}{C^0_{II}} \quad I = 1 \text{ to } 6, \text{ no sum} \quad (5)$$

$$D_{IJ} = \frac{\omega_{II}}{\omega^{\lim}_{IJ}} = \frac{C^0_{IJ} - C_{IJ}}{C^0_{IJ} + \text{sign}(C^0_{IJ} - C_{IJ})[C^0_{II}(1 - D_{II})C^0_{JJ}(1 - D_{JJ})]^{1/2}}$$

$$I, J = 1, \ldots, 6, I \neq J \quad (6)$$

3.3. Anisotropic damage tensor evolution

The variations of the stiffnesses C_{IJ} at each level of stress give the evolution of the damage tensor components D_{IJ} using Relations 5 and 6. These variations, Fig. 3, differ from one component to another and show clearly the anisotropy of the damage phenomenon. At failure, damage value is consequential, that

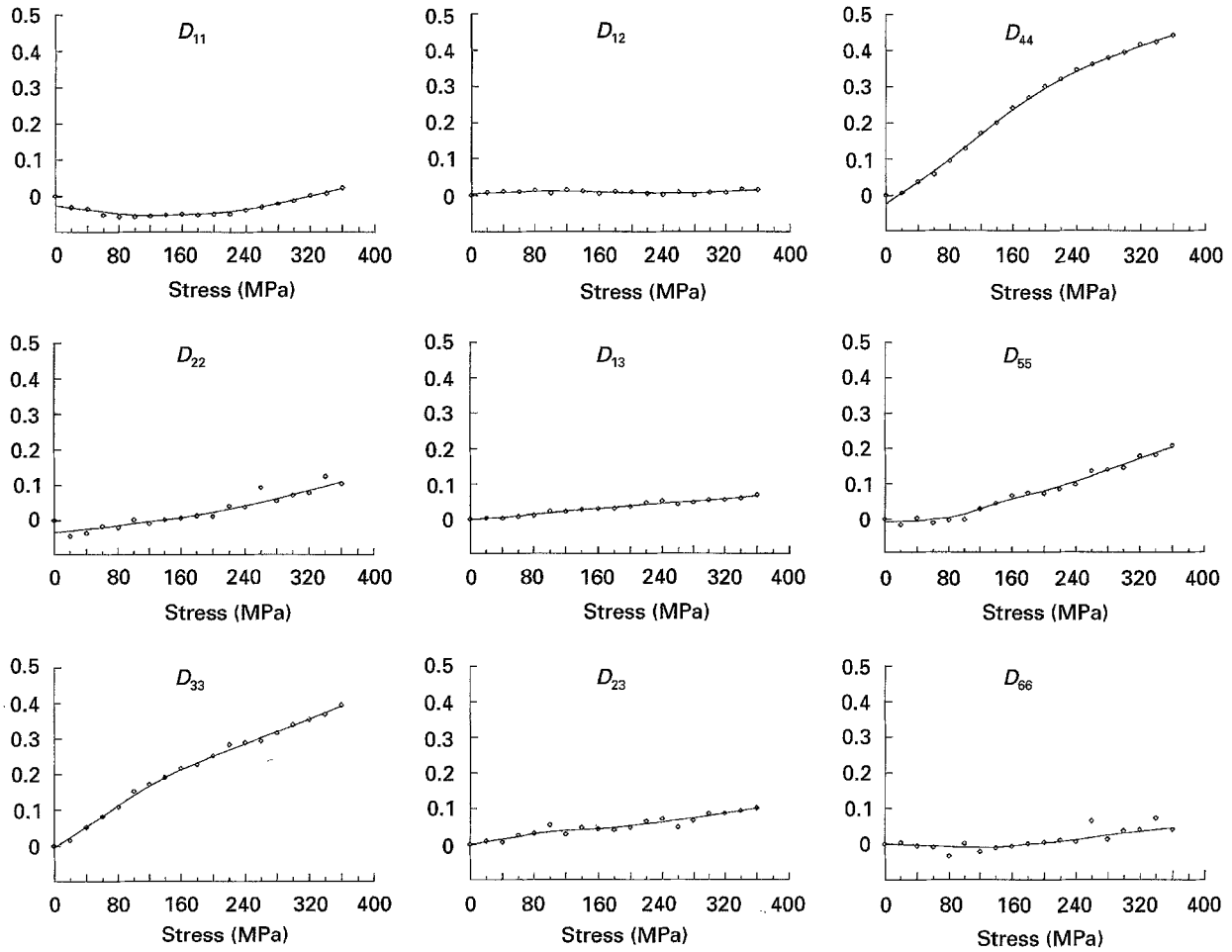

Figure 3 Evolution of damage tensor coefficients with the tensile stress in one of the fibre directions, direction 3, sample S0.

indicates the stiffness decrease associated to a distributed and generalized damage; the matrix multi-cracking. Extent of the damage is due to the substantial part of the matrix-to-composite total stiffness.

The damage parameter D_{33} associated with the stiffness in the tensile axis 3 exhibits an important linear increase. The level reached by the damage parameter connected with the inplane shear moduli ($D_{44} \approx 0.45$) is quite similar to the one reached by D_{33}. The non-zero components of the damage tensor are D_{33}, D_{44} and D_{55} relative to the planes that contain the loading direction. The other parameters relative to the plane normal to the tensile axis, D_{11}, D_{22} and D_{66}, do not vary significantly. This result is consistent with the analytical predictions of the effective elasticity tensor of an anisotropic solid containing penny-shaped cracks normal to the loading axis [15].

4. Stiffness tensor changes under 45° off-axis tensile loading

4.1. Rotation of coordinate axes

The effect of an off-axis solicitation is studied using sample S45, cut out at a 45° angle from the fibre axes, and loaded in this direction. Let R' (1', 2', 3') be the coordinate system associated with the sample S45 and R (1, 2, 3) the coordinate axes associated with the fibres, Fig. 4. Rotation of the coordinate system through a 45° angle about the $1 = 1'$ axis allows us to transform from one coordinate system to the other. The stiffnesses in the R' (1', 2', 3') coordinate system are C'_{ij} while C_{ij} are the stiffnesses in the R (1, 2, 3) coordinate system. C'_{ij} and C_{ij} are actually the components of the same tensor **C** in two different bases connected by a coordinate transformation matrix.

The carbon–SiC 2D composite presents initially in the R coordinate system a tetragonal symmetry with six independent stiffnesses. The R' coordinate axes are like elasticity principal axes. The orthotropic class of symmetry is retained in the R' (1', 2', 3') coordinate system and the stiffness matrix is:

$$[C'] = \begin{bmatrix} C'_{11} & C'_{12} & C'_{13} & 0 & 0 & 0 \\ C'_{12} & C'_{22} & C'_{23} & 0 & 0 & 0 \\ C'_{13} & C'_{23} & C'_{33} & 0 & 0 & 0 \\ 0 & 0 & 0 & C'_{44} & 0 & 0 \\ 0 & 0 & 0 & 0 & C'_{55} & 0 \\ 0 & 0 & 0 & 0 & 0 & C'_{66} \end{bmatrix}$$

For the sample S45 studied, the stiffnesses before loading measured in the R' (1', 2', 3') coordinate system are shown in Table I. In respect of the measurement accuracy, the directions 2' and 3' are symmetrically equivalent: $C'_{22} \approx C'_{33}$, $C'_{66} \approx C'_{55}$, $C'_{12} \approx C'_{13}$. The tetragonal symmetry remains in the $R'(1', 2', 3')$ coordinate axes.

On using the coordinate transformation matrix M, the stiffness matrix in the $R(1, 2, 3)$ coordinate system associated with the fibre directions becomes [27]:

$$[C] = [M][C'][M]^t$$

$$= \begin{bmatrix} C_{11} & C_{12} & C_{13} & C_{14} & 0 & 0 \\ C_{12} & C_{22} & C_{23} & C_{24} & 0 & 0 \\ C_{13} & C_{23} & C_{33} & C_{34} & 0 & 0 \\ C_{14} & C_{24} & C_{34} & C_{44} & 0 & 0 \\ 0 & 0 & 0 & 0 & C_{55} & C_{56} \\ 0 & 0 & 0 & 0 & C_{56} & C_{66} \end{bmatrix} \quad (7)$$

where $[M]^t$ designates the transpose of the matrix M:

$$[M] = \begin{bmatrix} 1 & 0 & 0 & 0 & 0 & 0 \\ 0 & a^2 & b^2 & c & 0 & 0 \\ 0 & b^2 & a^2 & -c & 0 & 0 \\ 0 & -c/2 & -c/2 & d & 0 & 0 \\ 0 & 0 & 0 & 0 & a & -b \\ 0 & 0 & 0 & 0 & b & a \end{bmatrix} \quad (8)$$

and $a = \cos\theta = 2^{1/2}/2$, $b = \sin\theta = 2^{1/2}/2$, $c = \sin 2\theta = 1$, $d = \cos 2\theta = 0$. The transformed elastic stiffnesses C_{ij} by clockwise rotation of coordinates through an angle 45° about the 1 axis are:

$$C_{11} = C'_{11}$$

$$C_{22} = C_{33} = \tfrac{1}{4}(C'_{33} + C'_{22}) + C'_{44} + \frac{C'_{23}}{2}$$

$$C_{12} = C_{13} = \tfrac{1}{2}(C'_{12} + C'_{13})$$

$$C_{23} = \tfrac{1}{4}(C'_{22} + C'_{33}) + \frac{C'_{23}}{2} - C'_{44}$$

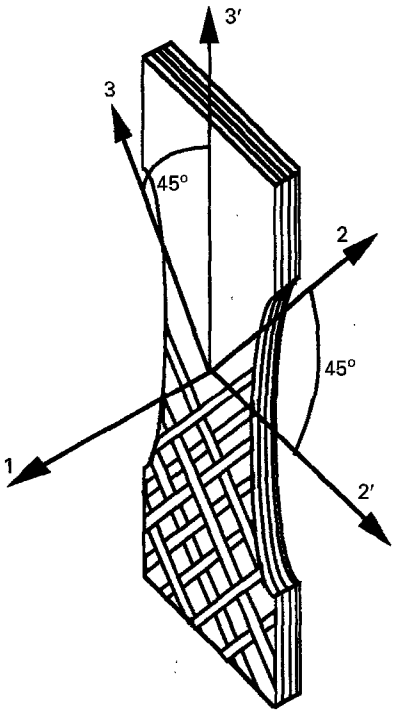

Figure 4 $R'(1', 2', 3')$ coordinate system associated to the sample S45, $R(1, 2, 3)$ the coordinate axes associated with the fibres.

TABLE I Initial stiffness coefficients (in GPa) and associated 90% confidence interval of the S45 sample measured in $R'(1', 2', 3')$, calculated in $R(1, 2, 3)$ by using the rotation transformation matrix and directly measured in (1, 2) plane of the system R that coincides with the (1, 45°) of the system R'

C'_{ij} measured in $R'(1', 2', 3')$	C_{ij} calculated in R (1, 2, 3)	C_{ij} measured in plane (1, 2)
$C'_{11} = 17 \pm 1$	$C_{11} = 17 \pm 1$	$C_{11} = 17 \pm 1$
$C'_{22} = 71 \pm 4$	$C_{22} = C_{33} = 99 \pm 8$	$C_{22} = 85 \pm 8$
$C'_{33} = 65 \pm 3$	$C_{66} = C_{55} = 11 \pm 0.2$	$C_{66} = 10.5 \pm 0.3$
$C'_{66} = 11.0 \pm 0.1$	$C_{44} = 19 \pm 5$	
$C'_{55} = 10.8 \pm 0.3$	$C_{12} = C_{13} = 2.4 \pm 0.4$	$C_{12} = 2.3 \pm 1.0$
$C'_{44} = 50 \pm 2$	$C_{23} = -1 \pm 8$	
$C'_{12} = 2.5 \pm 0.4$	$C_{14} = 0.1 \pm 0.4 \approx 0$	
$C'_{13} = 2.3 \pm 0.4$	$C_{24} = C_{34} = -1.5 \pm 2 \approx 0$	
$C'_{23} = 30 \pm 7$	$C_{56} = -0.1 \pm 0.2 \approx 0$	

$$
\begin{aligned}
C_{44} &= \tfrac{1}{4}(C'_{22} + C'_{33}) - \frac{C'_{23}}{2} \\
C_{66} &= C_{55} = \tfrac{1}{2}(C'_{66} + C'_{55}) \\
C_{14} &= \tfrac{1}{2}(C'_{12} - C'_{13}) \\
C_{24} &= C_{34} = \tfrac{1}{4}(C'_{33} - C'_{22}) \\
C_{56} &= \tfrac{1}{2}(C'_{55} - C'_{66}) \qquad (9)
\end{aligned}
$$

The initial stiffnesses C_{ij} calculated from Equation 9 in the $R(1, 2, 3)$ coordinate system by using the coordinate transformation matrix, are shown in Table I. Since the tetragonal symmetry remains in the $R'(1', 2', 3')$ coordinate axes, the tensile-shear coupling coefficients C_{14}, C_{24}, C_{34} and C_{56} are equal to zero with regard to the measurement accuracy. A way to validate the calculated stiffnesses C_{ij} is to compare them with those measured in the plane (1, 45°), Table I. This plane is a principal plane, since this sample exhibits a tetragonal symmetry. It coincides with the plane (1, 2) of the $R(1, 2, 3)$ coordinate axes.

The two samples, S0 and S45, have been cut out from different plates. The dispersion of the stiffness values measured is as important for samples cut of the same plate, as it is when taken out from different plates [24]. This variation is caused by the high sensitivity of the material properties to the porosity level and to the nonhomogeneous distribution of the porosity which is due to the manufacturing process [24].

4.2. Stiffness tensor changes in the 45° axes

Sample S45 has been submitted to an off-axis tensile test in the direction 3', until the sample failed at 170 MPa. Fig. 5 represents the variation of the elastic constants versus the σ'_3 applied stress measured with the hypothesis required by the ultrasonic technique that the material keeps its orthorhombic symmetry in the $R'(1', 2', 3')$ coordinate system [24]. The stiffness C'_{33} along the tensile axis strongly decreases, from 70 to 45 GPa. The degradation also affects the shear moduli C'_{44}, C'_{55} and C'_{66}. On the other hand, C'_{22} is essentially constant. These variations confirm that the cracks grow preferentially in the plane transverse to the loading direction 3'. The elastic symmetry, which was initially tetragonal, becomes increasingly orthorhombic in the (1', 2', 3') coordinate axes.

The damage parameters plotted in Fig. 6 are calculated using Equations 5 and 6 from the C'_{ij} stiffness changes in the R' (1', 2', 3') coordinate axes. The damage parameter D'_{33} associated with the stiffness in the tensile axis 3' reaches the value 0.3 when the fracture occurs. The parameter D'_{22} appears to be equal to zero considering its relative identification precision. The axis 3' tensile stress σ'_3 induces shear damage parameters D'_{44}, D'_{55} and D'_{66} that exhibit comparable values to that of D'_{33}.

Analysis of the matrix cracking, from the damage tensor variation plotted in Fig. 6, is more arduous than for the fibre directions tensile test. The microcracks appear more disordered because of the complication of the possible directions of cracks' growth. They may be determined by the bi-directional texture of the composite or determined by the applied stress direction. However, the cracks must grow preferentially in the plane transverse to the 3' loading direction since the damage D'_{33} associated to the stiffness in the tensile axis 3' exhibits an important increase while D'_{22} is quite equal to zero. Of course, this perpendicular to 3' loading direction matrix microcracking also affects the D'_{44} and D'_{55} damage parameters since three elasticity coefficients are always altered in the simple case of homogeneous distribution of parallel slit cracks [15].

Nevertheless, it is pointed out that the increases of both the damage parameters D'_{33} and D'_{44} become more weak beyond 120 MPa, while the components D'_{11}, D'_{55} and D'_{66} are still increasing. Microcracking of the matrix normal to the loading direction 3' seems to have reached a saturation level. Another degradation mechanism arises with a propagation direction which is not in the applied stress direction, or with a more disordered geometry.

4.3. Fully anisotropic degradation of the initially tetragonal symmetry

The change of the stiffnesses C_{ij} in the $R(1, 2, 3)$ coordinate system of the sample S45, calculated from the change of stiffnesses C'_{ij} in the R' (1', 2', 3') coordinate axes with the aid of Equation 9, are shown in Fig. 7. The loss of the tetragonal symmetry, since C'_{33} is no longer equal to C'_{22}, induces that the 2D carbon–SiC composite which presents a tetragonal symmetry with six independent stiffnesses, when submitted to a

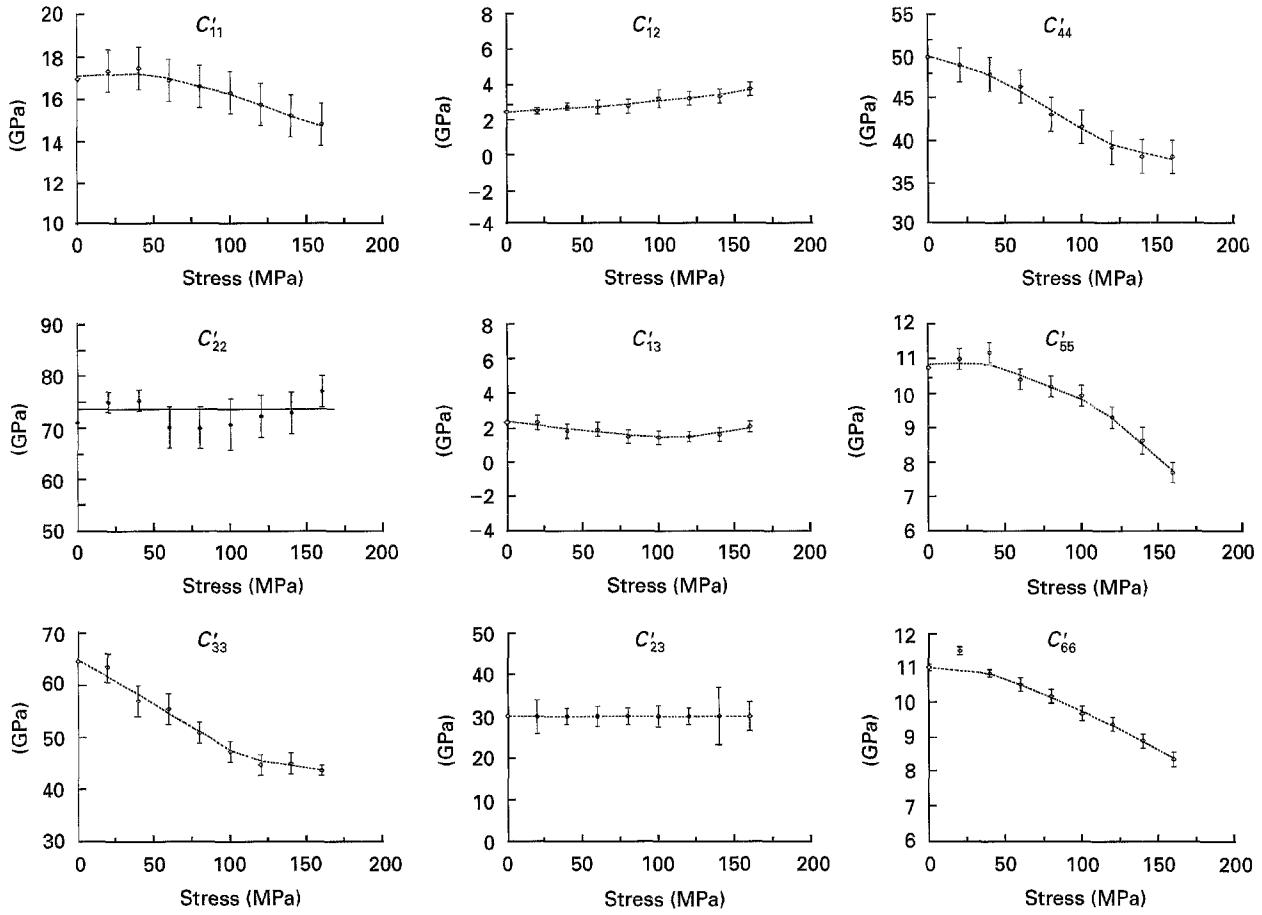

Figure 5 Variation of the stiffness tensor coefficients and their 90% relative confidence interval in the $R'(1', 2', 3')$ coordinate system, sample S45 submitted to a 45° off-axis tensile test.

complex stress, $[0, \sigma_2 = \sigma'_3/2, \sigma_3 = \sigma'_3/2, \sigma_4 = \sigma'_3/2, 0, 0]$ becomes increasingly monoclinic, with 13 independent elasticity coefficients, in the (1, 2, 3) coordinate axes. For the particular choice of rotation through an angle 45°, there are nine independent stiffnesses:

$$C_{IJ} =$$

$$\begin{bmatrix} C_{11} & C_{12} & C_{13} = C_{12} & C_{14} & 0 & 0 \\ & C_{22} & C_{23} & C_{24} & 0 & 0 \\ & & C_{33} = C_{22} & C_{34} = C_{24} & 0 & 0 \\ & & & C_{44} & 0 & 0 \\ & \text{sym} & & & C_{55} & C_{56} \\ & & & & & C_{66} = C_{55} \end{bmatrix}$$

In the $R'(1', 2', 3')$ coordinate system, C'_{12} remains close to C'_{13}. Similarly, the variations of C'_{55} and C'_{66} are quite identical. Consequently, the values of C_{14} and C_{56} remain weak. On the other hand, the initially zero tensile-shear coupling coefficients C_{24} and C_{34} have now become non-zero. These elasticity coefficients decrease continuously with the stress σ'_3 and reach the value of approximately -8 GPa when the fracture occurs. This points out a notable alteration of the elasticity symmetry due to the deterioration of the composite microstructure. The other non-diagonal coefficients are not affected by this damage process.

The variations of the stiffnesses C_{ij} in the $R(1, 2, 3)$ coordinate axes calculated from Equation 5 at each stress level give the evolution of the damage tensor components $\mathbf{D}_{IJ}$ in this coordinate system using Relations 5 and 6, Fig. 8. The damage parameters D_{22} and D_{33} are equal since the coordinate transformation gives $C_{22} = C_{33}$ for any stress level. It is in line with the fact that the directions 2 and 3 are submitted to the same tensile stress $\sigma_2 = \sigma_3 = \sigma'_3/2$. The decrease of the shear coefficients are consequent because of the superposition of the damage induced by the tensile stresses σ_2 and σ_3 and the shear stress $\sigma_4 = \sigma_{23} = \sigma'_3/2$.

The more noteworthy effect of the off-axis tensile solicitation in the direction 3′ is that the non-diagonal damage parameters D_{24} and D_{34} exhibit an increase of 0.2. This increase is due to the loss of the orthorhombic symmetry in the $R(1, 2, 3)$ coordinate system associated with the fibres. The off-axis tensile stress initiates microcracks that grow preferentially in the plane transverse to the loading direction 3′, Fig. 9. The predominant orientation of these cracks does not coincide with the fibre axes and induces a loss of symmetry [38]. This fully anisotropic elastic degradation is due to the anisotropic damage that affects

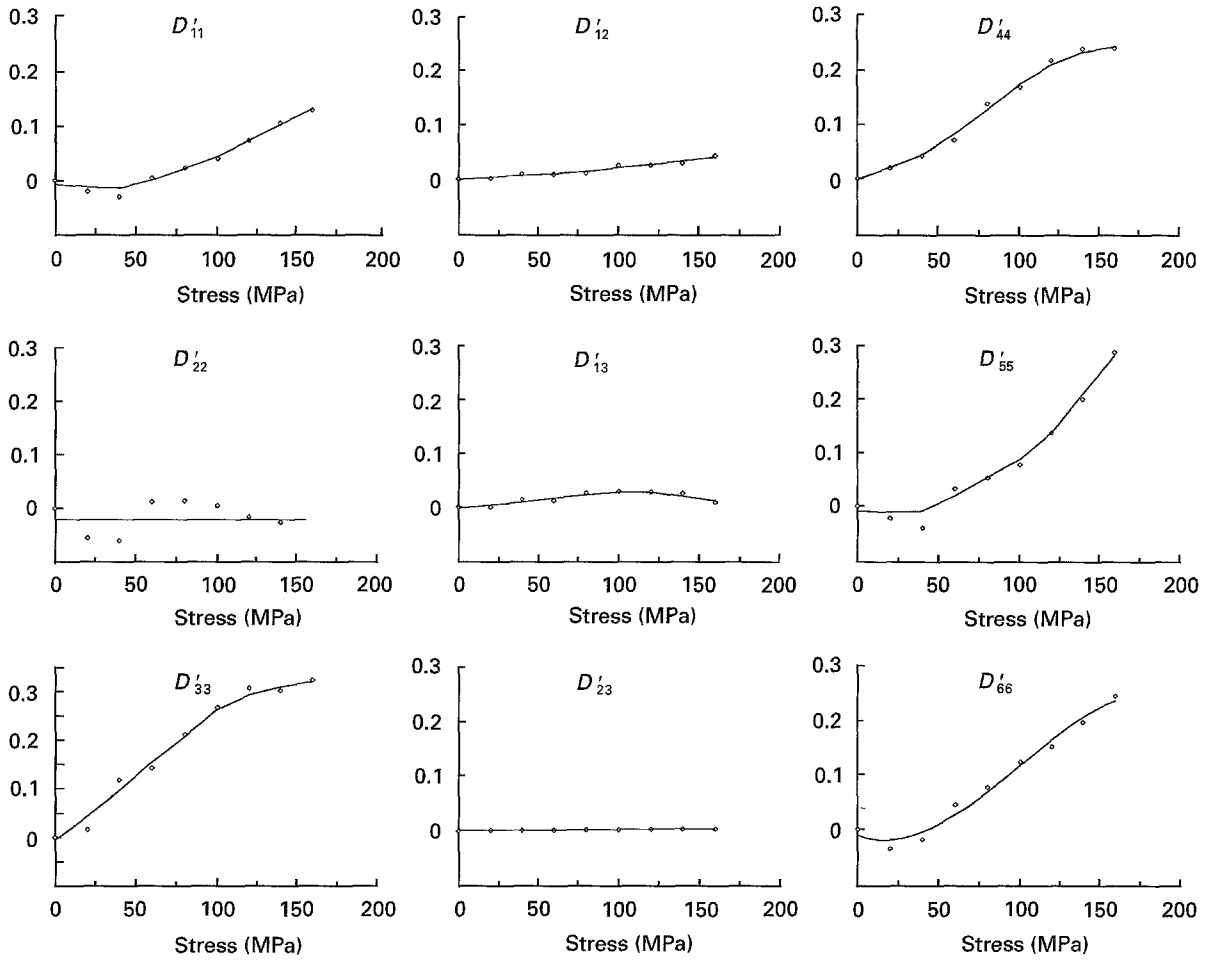

Figure 6 Evolution of damage tensor coefficients in the $R'(1', 2', 3')$ coordinate system, sample S45 submitted to a 45° off-axis tensile stress in direction 3'.

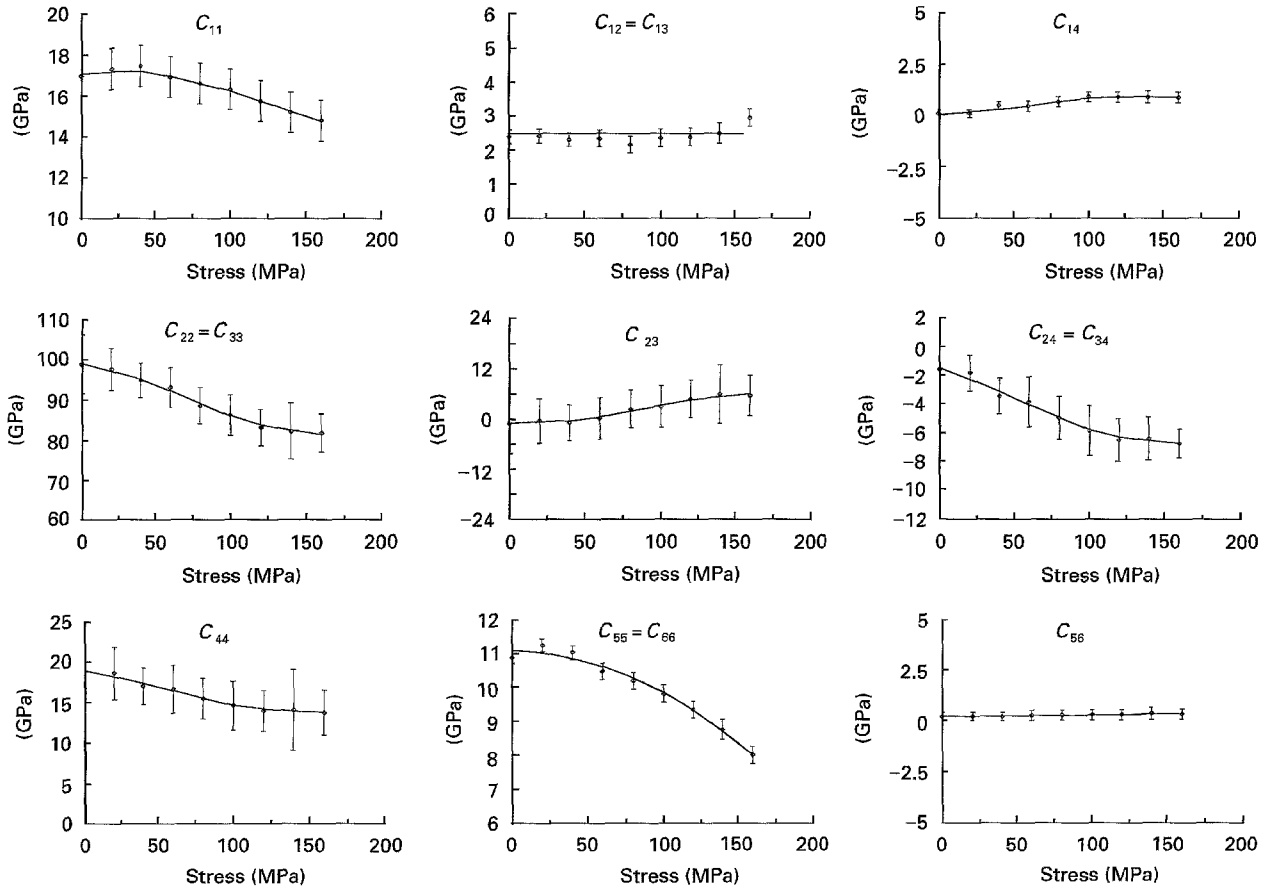

Figure 7 Variation of the stiffness tensor coefficients and their 90% relative confidence interval in the R (1, 2, 3) coordinate system, sample S45 submitted to a 45° off-axis tensile stress in direction 3'.

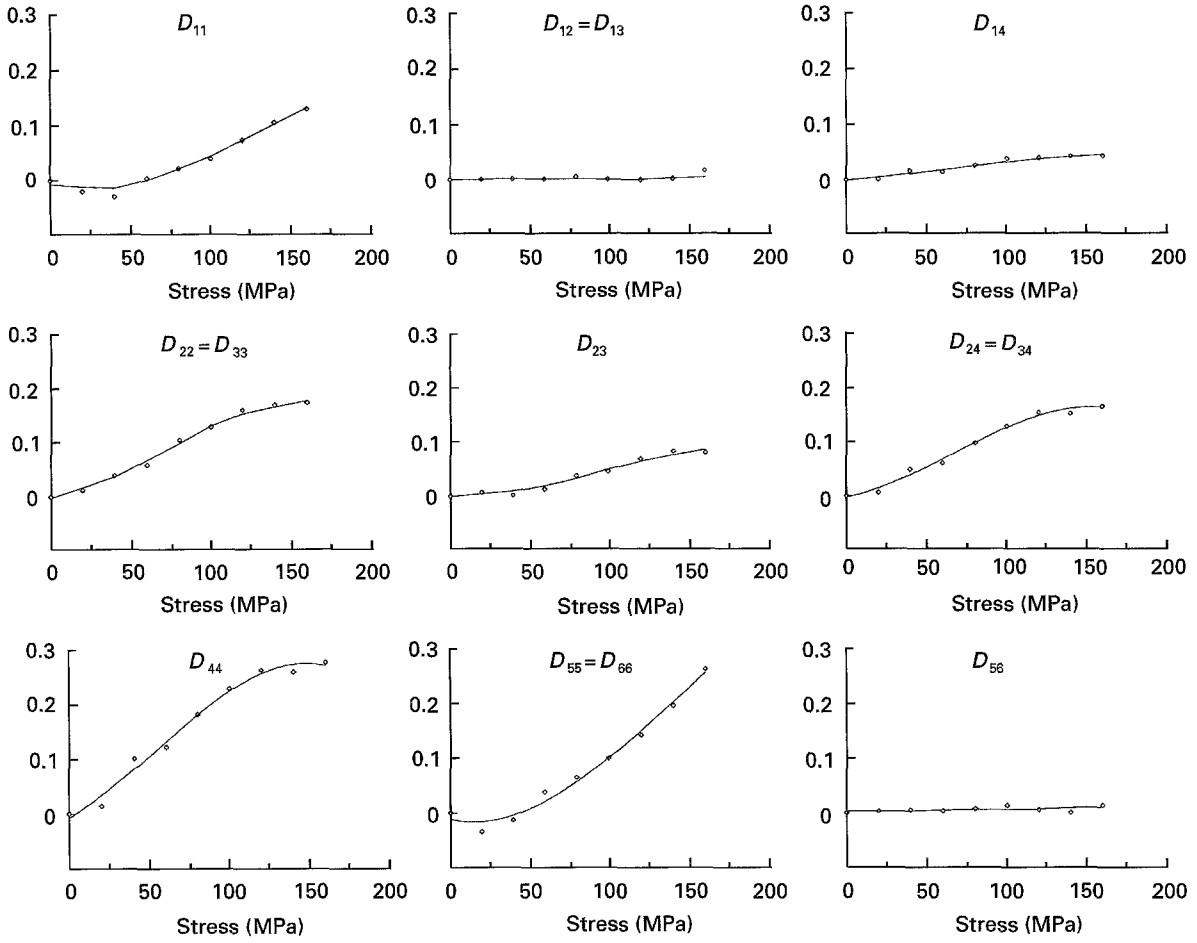

Figure 8 Evolution of damage tensor coefficients calculated in the R (1, 2, 3) coordinate system, sample S45 submitted to a 45° off-axis tensile test in direction 3'.

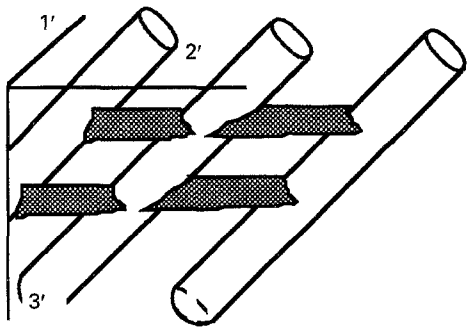

Figure 9 Microcracking of the matrix normal to the loading direction 3' in the sample S45 cutting out according to a 45° angle versus fibre directions.

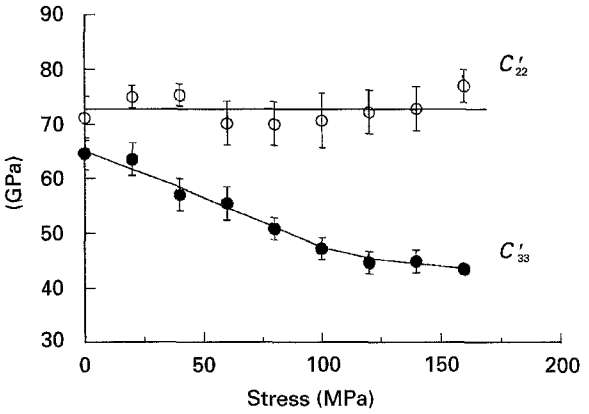

Figure 10 Induced anisotropy by off-axis tensile stress σ'_3.

differently the coefficients C'_{22} and C'_{33} that initially were quite equal, Fig. 10.

5. Conclusion

The development and the growth of microcracks highly affect the macroscopic behaviour of ceramic matrix composites. This deterioration is measured, at the macroscopic scale, by the changes of the material's stiffnesses. Since cracks have overriding propagation directions, the effect is highly anisotropic and the variations of the whole stiffness tensor must be studied. Because classical measurement methods lead to a partial identification of these tensor variations, an under load ultrasonic device is used making it possible to perform the measurements of stiffness tensor changes during a tensile test.

The measurements have been performed on a 2D woven carbon–SiC composite that presents a damaged elastic behaviour. The different variations of damage parameters characterize the anisotropy of the damaging process and justify the requirement of the independent identification of each stiffness coefficient. Comparison between measured stiffness change carried out without *a priori* crack geometry, and effective

elasticity coefficient predictions of a body containing cracks give the approximate orientation of crack systems.

When the composite is submitted to a tensile test in one of the fibre directions, the cracks grow preferentially in the plane transverse to the loading direction, with respect to the bi-directional texture of the composite. This degradation process preserves the orthotropic symmetry in the elastic coefficients since it is parallel to one of the three orthogonal axes of material symmetry. However, the predominant orientation of the microcracks destroys the balance of the carbon cloths. The elastic symmetry, which was initially tetragonal, becomes increasingly orthorhombic.

A tensile solicitation at 45° from fibre directions creates microcracks with a predominant orientation that does not coincide with the fibre axes, and induces a fully anisotropic elastic degradation. For this kind of degradation, the material effectively keeps its orthorhombic symmetry but the principal axes which remain mutually orthogonal, change their direction under load. So, in the coordinate axes associated with the fibres, the 2D carbon-SiC composite becomes monoclinic. The fully anisotropic degradation, that induces this loss of symmetry, is described by the non-diagonal damage tensor components D_{24} and D_{34}. These damage parameters take into account the coupling effects between the tensile stresses σ_2 and σ_3 and the shear stress σ_4.

The aim of this study was to prove the capability of the ultrasonic method to evaluate preferential orientation of matrix cracks comparative to the loading direction and to the natural axes of the composite. The very particular choice of an initially elastic tetragonal symmetry composite material, and of an off-axis angle of 45 degrees was imposed by the limiting hypothesis required by the ultrasonic technique that the material keeps its orthorhombic symmetry in an *a priori* known coordinate system.

The microcracking effect may be totally characterized when the response of a material to any stress has been measured. For that purpose, the wide area of off-diagonal solicitation must be investigated and the elasticity evaluation method must be improved to be able to characterize a fully anisotropic material, that means, a material that possesses no perpendicular planes of symmetry and exhibits a triclinic symmetry described with 21 independent stiffnesses.

Acknowledgement

This work was partially supported by Société Européenne de Propulsion under grant no. 479192.

References

1. J. AVESTON, G. A. COOPER and A. KELLY, in "Properties of fiber composites" (IPC Sci. and Tech. Press, Guildford, Surrey, 1971) pp. 15–24.
2. D. B. MARSHALL, B. N. COX and A. G. EVANS, *Acta Metall.* **33** (1985) 2013
3. D. B. MARSHALL and A. G. EVANS, *J. Amer. Ceram. Soc.* **68** (1985) 225
4. G. BERHNART, P. LAMICQ and J. MACE, *Ind. Céram.* **790** (1985) 51.
5. B. BUDIANSKY, J. HUTCHINSON and A. G. EVANS, *J. Mech. Phys. Solids* **34** (1986) 167.
6. L. S. SIGL and A. G. EVANS, *Mech. Mater.* **8** (1989) 1.
7. P. G. CHARALAMBIDES and A. G. EVANS, *J. Amer. Ceram. Soc.* **72** (1989) 746.
8. B. BUDIANSKY and R. J. O'CONNEL, *Int. J. Solids Struct.* **12** (1976) 81.
9. A. HOENIG, *ibid.* **5** (1979) 137.
10. E. T. ONAT, *Int. J. Eng. Sci.* **22** (1984) 1013.
11. H. HORII and S. NEMAT-NASSER, *Int. J. Solids Struct.* **21** (1985) 731.
12. *Idem, ibid.* **21** (1985) 731.
13. C. T. HERAKOVICH, J. ABOUTI, S. W. LEE and E. A. STRAUSS, *Mech. Mater.* **7** (1988) 91.
14. N. LAWS and G. J. DVORAK, *Int. J. Solids Struct.* **23** (1987) 1269.
15. N. LAWS, G. J. DVORAK and M. HEJAZI, *Mech. Mater.* **2** (1983) 123.
16. R. TALREJA, *J. Compos. Mater.* **19** (1985) 355.
17. L. DAVISON and A. L. STEVENS, *J. Appl. Phys.* **44** (1973) 668.
18. D. KRAJCINOVIC and G. U. FONDEKA, *J. Appl. Mech.* **48** (1981) 809.
19. S. MURAKAMI and N. OHNO, in "Creep in Structures", edited by A. R. S. Ponter and D. R. Hayhust (Springer, Berlin, 1981) pp. 922–44.
20. J. BETTEN, *J. Méc. Théor. Appl.* **2** (1983) 13.
21. A. LITEWKA, *Arch. Mech.* **37** (1985) 631.
22. S. BASTE and B. AUDOIN, *Eur. J. Mech. A/Solids* **10** (1991) 587.
23. B. AUDOIN and S. BASTE, in "Composites, Design, Manufacture and Applications", ICCM 8, Honolulu, July 1991, edited by S. W. Tsai and G. S. Springer (Ed SAMPE, Covina, CA, 1991) pp. 39-C-1-39-C10.
24. *Idem, J. Appl. Mech.* **61** (1994) 309.
25. Z. G. WANG, C. LAIRD, Z. HASHIN, B. W. ROSEN and C. F. YEN, *J. Mater. Sci.* **26** (1991) 4751.
26. J. ROUX, in IEEE 1990 Ultrasonics Symposium, Honolulu, December 1990 (IEEE, New York, 1990) pp. 1065–73.
27. B. A. AULD, Acoustic fields in solids, Vol. 1 (Wiley-Interscience, New York, 1973).
28. B. CASTAGNÈDE, J. T. JENKINS, W. SACHSE and S. BASTE, *J. Appl. Phys.* **67** (1990) 2753.
29. S. BASTE and B. HOSTEN, *Rev. Phys. Appl.* **25** (1990) 161.
30. B. HOSTEN, *Ultrasonics* **30** (1992) 365.
31. M. F. MARKHAM, *Composites* **1** (1970) 145.
32. J. B. WALTER, L. A. LOTT and K. L. TELSCHOW, in "Review of Progress in Quantitative NDE", edited by D. O. Thompson and D. E. Chimenti (Plenum Press, New York, 1988) pp. 971–978.
33. B. AUDOIN and J. ROUX, *Revue Phys. Appl.* **25** (1990) 1011.
34. B. AUDOIN, S. BASTE and B. CASTAGNÈDE, *C. R. Acad. Sci. Paris* **II312** (1991) 679.
35. D. KRAJCINOVIC, *Mech. Mater.* **8** (1989) 117.
36. M. ORTIZ, *ibid.* **4** (1985) 67.
37. J. LEMAITRE and J. L. CHABOCHE, *J. Mech. Appl.* **2** (1978) 167.
38. R. TALREJA, *Proc. Roy. Soc. Lond.* **A399** (1985) 195.

Received 13 June 1994
and accepted 19 September 1995